INVERSE IDENTIFICATION OF TRANSIENT THERMAL PROPERTIES AND HEAT SOURCES USING GENETIC ALGORITHMS

A Thesis

Presented to the Faculty of the Graduate School

of Cornell University

In Partial Fulfillment of the Requirements for the Degree of

Master of Science

by

Sanford Waldo Phillips

August 2006

ABSTRACT

This work investigates the solution to inverse problems in heat transfer using genetic algorithms. Genetic algorithms are robust, stochastic search techniques which also admit the ability to search highly nonlinear problems. In this work, computational techniques are developed for the simultaneous inverse identification the internal heat generation and the thermal diffusivity of early age concrete as functions of time, as well as constant convective coefficients. Through the use of several numerical examples it is shown that this methodology yields accurate results for the inverse heat transfer problem in finding several unknown conditions simultaneously.

BIOGRAPHICAL SKETCH

Sanford Phillips was born and raised in Randolph, VT where he attended Randolph Union High School. He received his undergraduate degree in May 2004 from Johns Hopkins University in Baltimore, MD.

Dedicated to my parents George and Elizabeth Phillips

ACKNOWLEDGMENTS

Many thanks to Drs. Wilkins Aquino and William Chirdon for their invaluable help. The author would like to acknowledge the Cornell Theory Center for use of its computational resources without which this research would have been impossible. Thanks to Cornell Engineering Learning Initiatives who provided assistantship for part of this degree.

TABLE OF CONTENTS

LIST OF FIGURES

LIST OF TABLES

LIST OF SYMBOLS

Nomenclature

a_j	A point on the parameterized thermal diffusivity curve
δ	Magnitude of the noise
g_j	A point on the parameterized heat generation curve
λ_1	The first-order Tickhonov regularization parameter
$\{\vec{M}\}$	The set of parameters, p_i
p_i	A normalized parameter found by the algorithm
p_i^{target}	A normalized target parameter value
$p_i^{'}$	A parameter which as been changed for the next generation
Π_i	A non-normalized parameter value
$T^{MEA}(\vec{x},t)$	Measured target temperatures
$T_{t,s}^{error}$	Temperature including error
$T_{t,s}^{exact}$	Simulated temperature
υ	A random variable for noise generation
Υ_j	A scaling factor
$\phi_j(t)$	A basis function

Physical Quantities

$\alpha(t)$	Transient thermal diffusivity $\left(m^2/s\right)$
$B_i(t)$	Biot number
$\gamma(t)$	Transient heat generation $\left(K/s\right)$
η	Modified convection coefficient $\left(m/s\right)$
L_c	Characteristic length (m)

T	Temperature (K)
T_e	Temperature of the environment (K)
t	Time (s)
$\underset{\sim}{x}$	Spatial coordinate (m)

Finite Element Symbols

$[B]$	Matrix of derivatives of $[N]$
Γ	Boundary of Ω
Γ_q	Portion of the boundary where convective boundary conditions are specified
Γ_T	Portion of the boundary where essential boundary conditions are specified
$[C]$	Heat capacity matrix
e	Indicates the element domain
$\{F(t)\}$	Convection heat flux vector
$\{G(t)\}$	Heat source vector
$[H]$	Surface convection matrix
$\underset{\sim}{n}$	Unit vector normal to the boundary
$[K(t)]$	Thermal diffusivity matrix
$[N]$	Matrix of interpolation functions
T_0	Initial temperature field
Ω	Domain of interest

Quantities

q	Number of sensors
r	Number of parameters

z	Number of time steps
n	Number of runs done

Equations Defined

$E\left[\gamma(t),\alpha(t),\eta\right]$	Error functional acting on parameter functions.
$T^{FEA}\left(\vec{x},t,\alpha(t),\gamma(t),\eta\right)$	The solution to the direct problem using finite element analysis
$E_p(\vec{M}_i)$	Parameter error measure
$E_T(\vec{M}_i)$	Temperature error measure
$\max(T)$	Maximum temperature at any sensor at any time step

CHAPTER 1

THE INVERSE AND FORWARD MODELS

Introduction

Traditional heat transfer problems involve the calculation of a temperature field based on known initial conditions, boundary conditions and material thermal properties. Calculation of temperatures in the body based on these properties is called the Direct Heat Transfer Problem (DHTP). This work focuses on the Inverse Heat Transfer Problem, (IHTP) where initial conditions, boundary conditions or material thermal properties are inferred based on transient temperature fields. The aim of an inverse problem is to "infer the causes from the effects". Unlike the DHTP, the IHTP may exhibit non-unique solutions, or may be unstable with respect to the input data, conditions which make the IHTP ill-posed.

Inverse problems in heat transfer are of general engineering interest, applications include quality control of early age concrete [1], remote sensing, and damage identification [2]. An influential early work in inverse heat transfer was done in [3], where Giedt investigated the temperatures on the interior surface of a gun barrel during firing. Since it was impossible to measure the interior temperatures directly, indirect measurements were used and the interior temperatures were inversely determined. Much of the work in IHTP has been focused on the estimating a single unknown function; Su et. al, and Truffart et. al. [4, 5] used inverse techniques to investigate transient modified convection coefficients, Al-Najem and Abou et. al. [6, 7] searched for unknown internal heat generation functions, and Jang et. al. [8] searched for unknown boundary heat fluxes, notable exceptions are Rodrigues et.al.

who searched for both diffusivity and heat generation as spatial functions and Silva et. al who identified only heat generation, but searched for variations in both time and space [9, 10]. Modern methods in these problems involve formulating the problem as a functional minimization problem and use a gradient-based minimization technique (see for example [4-8]). To lower the computation cost of evaluating the gradient for minimization, Su. el. al. and Abou. et. al formulated the adjoint problem to analytically determine the gradient of the error functional [4, 7].

This work presents a methodology for solving the IHTP which differs from previous reported work in two key areas. First, this work shows that transient thermal properties can be inferred simultaneously with boundary conditions which are constant. Second, the work presented here uses a genetic algorithm to minimize the error functional; this alleviates the disadvantages of gradient-based approaches, which may become trapped in local minima and require the existence of the gradient, which may also be difficult to calculate.

The work most similar to this thesis is presented in a journal paper by Rodrigues, Orlande and Dulikravich and a conference proceeding by Colaço, Orlande, Dulikravich and Rodrigues [9, 11]. They presented a method for simultaneously identifying thermal diffusivity and heat generation for a non-homogenous material. In addition to the differences mentioned above, this work differs from the results they presented in two key areas. First, Rodrigues et. al. assumed a non-homogeneous material with temporally-constant material properties; the present work assumes homogenous material with transient material properties. The second key difference is that this work investigates the effect of 2D effects in the temperature field, while Rodrigues et. al. presented only 1D examples.

The main goal of this work is to investigate the feasibility of simultaneously estimating transient thermal properties, heat generation, and convective boundary coefficients from sparse temperature measurements. A secondary goal is to show that simultaneous identification of internal heat generation and thermal diffusivity is possible using just surface temperature measurements. The effect of sensor layout, noise, and simultaneous estimation of different parameters on the accuracy of the solution is presented. First the DHTP problem is formulated, along with the finite element (FE) formulation. Next the IHTP is presented, and two error measures are derived. The genetic algorithm is introduced next, with specific discussion of the particular algorithm used in this work. Lastly several numerical examples are presented, which illustrate the abilities and limitations of the presented methodology.

Formulation of the Problem

The inverse identification of thermophysical properties can be broken into two main problems: the direct problem, usually solved with numerical methods such as finite elements, boundary elements, finite differences, finite volume methods, etc., and the inverse problem, which is cast as an optimization problem and, in this work, is solved using genetic algorithms.

The Direct Problem

Consider a 3D domain Ω and its boundary Γ, for problems where thermal diffusivity and heat generation are functions of time and the material is considered to be homogeneous and isotropic. The heat conduction initial boundary problem can be described through the governing energy equation

$$\frac{\partial T}{\partial t} = \nabla \cdot \alpha(t) \nabla T + \gamma(t), \quad \underline{x} \in \Omega, \quad t \in [0, t_{\max}], \tag{1}$$

boundary conditions

$$\alpha(t)\nabla T\cdot\vec{n}=\eta\left(T_e-T\right),\quad \text{on } \Gamma_q, \tag{2}$$

$$T\left(\vec{x},t\right)=T\left(\vec{x}\right),\quad \text{on } \Gamma_T, \tag{3}$$

$$\Gamma_q \cup \Gamma_T=\Gamma, \tag{4}$$

$$\Gamma_q \cap \Gamma_T=\varnothing, \tag{5}$$

and initial condition

$$T\left(\vec{x},0\right)=T_0\left(\vec{x}\right). \tag{6}$$

In the above equations, T is temperature, t is time, $\vec{x}$ is a spatial position vector, $\alpha(t)$ is the thermal diffusivity, $\gamma(t)$ is a heat generation source term, η is the modified convection coefficient, $\vec{n}$ is the unit vector normal to the boundary Γ, T_e is the temperature of the environment, Γ_q is the part of the boundary where convective boundary conditions are specified, Γ_T is the part of the boundary where essential boundary conditions are specified, and T_0 is the initial temperature field.

In all but the most trivial cases, numerical methods are required to obtain approximate solutions to Equations (1)-(6). In this work, the finite element method was used. It can be shown that, through finite element discretization, the initial boundary value problem described above reduces to a system of ordinary differential equations expressed as [12]

$$[C]\{\dot{T}\}+\left([K(t)]+[H]\right)\{T_g\}=\{F(t)\}+\{G(t)\}, \tag{7}$$

where

$$[C]=\sum_{elements}\int_{\Omega^e}[N]^T[N]\,d\Omega^e, \tag{8}$$

the thermal diffusivity matrix is

$$[K(t)] = \sum_{elements} \int_{\Omega^e} \alpha(t)[B]^T[B]\, d\Omega^e \,, \tag{9}$$

the surface convection matrix is

$$[H] = \sum_{elements} \int_{\Gamma^e} \eta[N]^T[N]\, d\Gamma^e \,, \tag{10}$$

the convection heat flux vector is

$$\{F(t)\} = \sum_{elements} \int_{\Gamma^e} [N]^T \eta\, T_e(t)\, d\Gamma^e \,, \tag{11}$$

and the heat source vector is

$$\{G(t)\} = \sum_{elements} \int_{\Omega^e} [N]^T \gamma(t)\, d\Omega^e \,. \tag{12}$$

In the above equations, $[N]$ is the matrix of interpolation functions, $[B]$ is a matrix containing the derivatives of the shape functions with respect to spatial coordinates, and the superscript e indicates element domain. The above system of ordinary differential equations was integrated in this work using the backward Euler time integration scheme.

Formulation of the Inverse Problem

The inverse problem consists of identifying the modified convection coefficient, thermal diffusivity, and heat generation in Equations (1) and (2) from temperatures measured at a set of q sensors $\left(x_1 \mathrm{K}\ x_q\right)$ over a time interval $[0, t_{\max}]$ and can be described as follows. The functions $\gamma(t)$ and $\alpha(t)$ are assumed to belong to the space $H^1(0,t_0)$, defined as $H^1(0,t_0) = \left\{ f(t) : \int_0^{t_0} f(t)^2 + \left(\frac{df(t)}{d(t)} \right)^2 dt < \infty \right\}$.

Defining the error functional

$$E\left[\gamma(t), \alpha(t), \eta\right] = \int_0^{t_{\max}} \sum_{i=1}^{q} \left[T^{FEA}\left(\vec{x}_i, t, \alpha(t), \gamma(t), \eta\right) - T^{MEA}\left(\vec{x}_i, t\right) \right]^2 dt \,, \tag{13}$$

the inverse problem is cast as an optimization problem as

$$\underset{\substack{\gamma(t),\alpha(t)\in H^1(0,t_{\max}) \\ \eta\in \mathrm{i}}}{\text{minimize}} \left[\mathrm{E}\left(\gamma(t), \alpha(t), \eta\right) \right]. \tag{14}$$

In Equation (13), $T^{FEA}\left(\vec{x},t,\alpha(t),\gamma(t),\eta\right)$ is the solution of the direct problem evaluated through finite element analysis and $T^{MEA}\left(\vec{x},t\right)$ is the measured temperature field. In this work the functions $\gamma(t)$ and $\alpha(t)$ are parameterized using a finite dimensional basis, $\phi_j(t), j = 1\text{K}\ m$, as

$$\gamma(t) = \sum_{j=1}^{m} g_j \phi_j(t) \tag{15}$$

and

$$\alpha(t) = \sum_{j=1}^{m} a_j \phi_j(t) \tag{16}$$

Where g_j and a_j are the values of heat generation and thermal diffusivity at time step j, respectively. In this work, the basis functions

$$\phi_j(t) = \begin{cases} \dfrac{t - t_{j-1}}{t_j - t_{j-1}} & t_{i-1} \le t < t_i \\ 1 - \dfrac{t - t_j}{t_{j+1} - t_j} & t_i \le t < t_{i+1} \\ 0 & otherwise \end{cases} \tag{17}$$

were used.

By introducing the above parameterization, the problem defined in Equation (14) becomes a finite dimensional optimization problem that can be expressed as

$$\underset{\vec{M} \in R^m}{\text{minimize}} \left[E_T\left(\vec{M}\right) \right], \tag{18}$$

where a parameterized version of the error functional in Equation (13) for z time steps, and q sensors is expressed as

$$E_T\left(\vec{M}\right) = \frac{1}{z+q} \sum_{s=1}^{p} \sum_{i=1}^{q} \left[T^{FEA}\left(\vec{x},t_s,\vec{M}\right) - T^{MEA}\left(\vec{x},t_s\right) \right]^2 \tag{19}$$

In the above equations, $\vec{M}$ is a vector that contains the unknown parameters a_j, g_j, and η, $E_T\left(\vec{M}\right)$ is referred to as the temperature error.

An additional error measure is defined to estimate the quality of the solution in the numerical experiments that will be presented in the next section. This error measure is defined as

$$E_p(\overset{\mathrm{r}}{M}) = \frac{1}{r}\sum_{i=1}^{r}(p_i - p_i^{target})^2 \ , \tag{20}$$

where p_i^{target} are the r normalized target parameters which were used to generate the experimental temperature measurements, and p_i is a parameter found by the algorithm, this is referred to as the parameter error.

Regularization

Inverse problems are often ill-posed in the sense that non-unique solutions may exist, and the solution may be sensitive to errors in the input data (i.e. instability). The former was partially addressed in this work by using a larger number of measurements than parameters to be identified in order to constrain the solution. However, it is important to bear in mind that this still does not guarantee uniqueness and different executions must be used to estimate the possibility of non-unique solutions. Whether or not an inverse problem is ill-posed is very often difficult to determine *a priori*. The stability pathology was addressed by using first-order Tikhonov regularization [13] as

$$\begin{aligned} E\left[g(t),k(t),h\right] = \int_0^{t_{\max}} \sum_{i=1}^{q}\left[T^{FEA}\left(\overset{\mathrm{r}}{x},t,k(t),g(t),h\right) - T^{M}\left(\overset{\mathrm{r}}{x},t\right)\right]^2 dt + \\ \lambda_1 \int_0^{t_{\max}} \left(\left|\frac{dg(t)}{dt}\right|^2 + \left|\frac{dk(t)}{dt}\right|^2\right) dt \end{aligned} \tag{21}$$

where λ_1 is the regularization parameter. The Tikhonov regularization described in the above equation penalizes functions with drastic oscillations. In this work, it was found that $10^{-3} \geq \lambda_1 \geq 10^{-5}$ produced satisfactory results, which agree with values reported in [14].

CHAPTER 2

SOLUTION TO THE INVERSE HEAT TRANSFER PROBLEM USING GENETIC ALGORITHMS

Overview of Genetic Algorithms

Genetic Algorithms (GA) are a form of evolutionary search, which mimic the process of the evolution of an organism and can be used to solve a wide variety of problems in engineering and science. GA were proposed by Holland in 1975 and have been used extensively in engineering problems [15-18]. To use a genetic algorithm, the problem to be solved is parameterized; a full set of parameters is considered a chromosome. In each iteration of the algorithm, a set of chromosomes, called a population, is affected by evolutionary forces such as selection, random mutation, and the creation of hybrid genetic offspring through crossover.

The algorithm chooses chromosomes through a process which emulates natural selection with a fitness or objective function as the surrogate for the natural environment. In producing the next generation, pairs of individuals from the current population are selected based on their fitness to serve as parents. Operators such as crossover and mutation are crucial in genetic algorithms and are used to produce new individuals. The crossover operation relates to the exchange of genetic information between parents, while the mutation operator relates to random changes in the individuals, promoting the exploration of diverse areas of the search space and preventing the evolutionary process from getting trapped in mediocre solutions (i.e. local minima).

Genetic algorithms are attractive for complex optimization problems because of their inherent advantages such as parallelism, convergence to global optima, adaptation, and the lack of need for the gradient of the error functional. In addition, genetic algorithms are less sensitive than gradient-based optimization methods to the distance between an initial guess and the global optimum. More detailed information on genetic algorithms can be found in References [19, 20].

Specific Genetic Algorithm Used in This Work

In this work, the optimization problem defined in Equation (17) was solved using genetic algorithms. A crucial aspect in the use of genetic algorithms is how solutions are represented. In this work, the parameters in $\{\overset{\mathrm{r}}{M}\}$ were encoded in strings of real numbers. The first m numbers represented the heat generation parameters, the next n parameters corresponded to the thermal diffusivity function, and the last r numbers represent modified convection coefficients. Each string represents a potential solution to the inverse problem at hand.

The process is shown schematically in Figure 1. Initially, random parameter sets, representing internal heat generation, thermal diffusivity, and modified convection coefficients are each evaluated by the objective function. The objective function runs a forward-analysis using a finite element program and calculates the error. The objective function then returns the fitness, which, in this work, is the algebraic inverse of the error. Once each of the parameter sets has been assigned a fitness it is operated on by the standard GA mechanisms of crossover, mutation and natural selection.

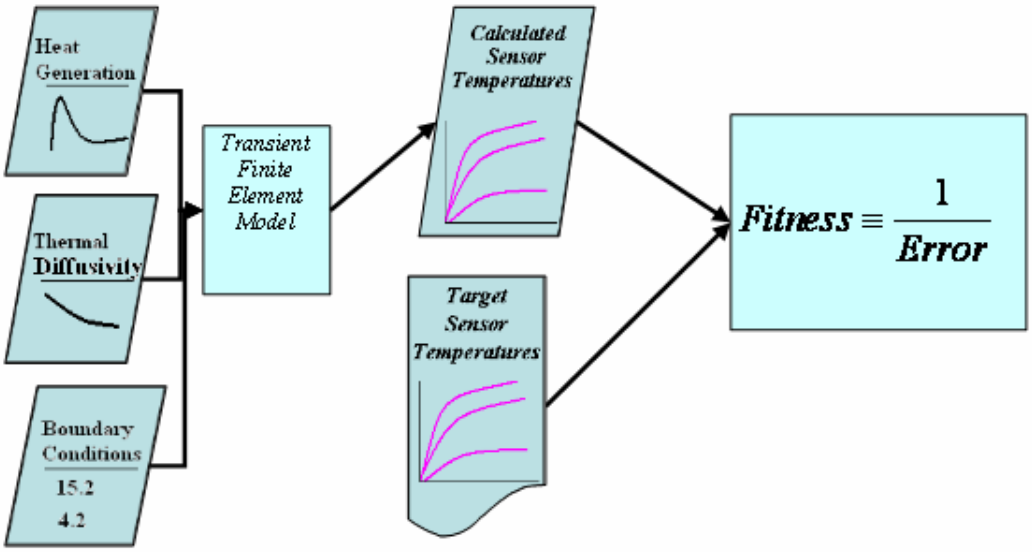

Figure 1 Overview of the objective function.

One difficulty sometimes encountered in the formulation of a real-valued GA is how mutation affects parameters which have significantly different scales. For instance, a point on the heat generation curve may have a value on the order of $10^{-3} - 10^{-1}\ {}^{K}\!/_{s}$, while a point on the diffusivity curve may have a value of $10^{-9} - 10^{-7}\ {}^{m^2}\!/_{s}$, the large difference in the values of each parameter can make it difficult for the mutation operator to scale initially random values up and down to be within a physically reasonable range. To combat this problem, the genetic algorithm was formulated to work with real valued numbers in the range $[0,1]$. Each parameter was then scaled by the finite element program into the appropriate range. When creating target parameter sets, each parameter value in the target chromosomes was scaled so that $p_i \in [0, 0.85]$. The parameter p_i represents an entry in a solution chromosome (i.e. diffusivity parameter, heat generation parameter, or modified convection coefficient). The reason for choosing larger bounds for the GA search space was to avoid parameters which fall at the ends of the search range, which makes the problem harder for the GA.

Selection Function

Rank-based selection is used in this algorithm. The new population is chosen from the old based on the rank, the highest fitness member in the old population is rank #1, the second-best solution is rank #2, etc. Seventy percent of the new population is chosen from the top thirty percent of the old population, and the other thirty percent chosen from the bottom seventy percent. This ensures that selective pressure increases the overall average fitness, while maintaining genetic diversity.

Crossover

Two-point crossover is used, with 50% of the members of the new population (on average) composed of parts of two parent chromosomes. The two point cross over technique is illustrated in Figure 2.

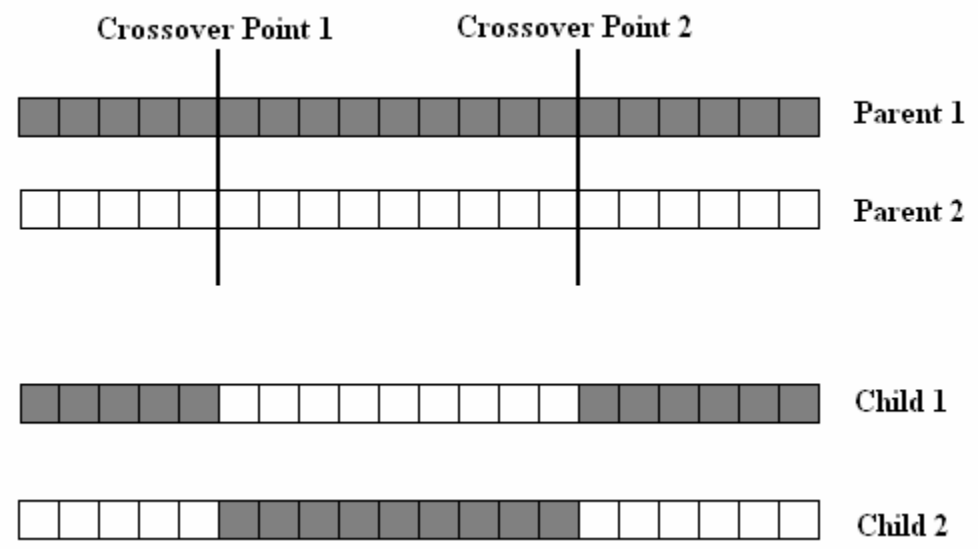

Figure 2 Schematic of two-point crossover

Two points are randomly chosen along the length of the chromosome, the parameters between those two points are then swapped on each parent chromosome to make the two children. Additionally, with 25% probability the two crossover points are both chosen to be directly in the middle.

Mutation

Random mutation is used to introduce diversity into the population and ensure the entire parameter space was searched. Each parameter in each chromosome has probability of being mutated of $1/r$ where r is the number of parameters in each chromosome, thus on average each chromosome has one mutation, but some may have none and some may have more than one. The mutation function replaces the initial value of a parameter, p_i with a new value, p_i'. With 35% probability p_i' is uniformly distributed in $(0,1)$. With 65% probability p_i' is chosen such that,

$0.75 * p_i \le p_i' \le 1.25 * p_i,\ p_i' \le 1$

p_i' is uniformly distributed in that range. The first condition is normal random mutation, the second is a "nudge" mutation which allows the GA to incrementally converge to exact values and increases the ability of the algorithm to search the 'edges' of the parameter space.

CHAPTER 3

NUMERICAL EXAMPLES

Introduction

The algorithm was tested with several target parameter sets, different sensor arrangements, regularization types, noisy target data, and different models. Genetic algorithms are stochastic search processes. Thus, to draw conclusions, multiple runs must be considered. In each of the examples presented here, 10 runs were performed with different initial random seeds. In all cases presented here, a set of target parameters were used to generate target temperatures at a group of sensors, the genetic algorithm then searched the parameter space starting from initially random points to find parameter sets which produced temperatures which most closely matched the target temperatures. The numerical simulations were performed with finite element analysis, mesh and temporal convergence was checked to ensure the models were accurate.

The target system chosen as the base for numerical experiments was a Styrofoam cylinder containing early age concrete, the properties of the system were chosen to loosely emulate the experimental setup reported by Lautz [1]. The geometry presented by Lautz used as a base here is shown in Figure 3. Two versions of this geometry were considered, a 1D version was used for the majority of the tests and a 2D axisymmetric model for others. In both models of the geometry, only the concrete portion was modeled.

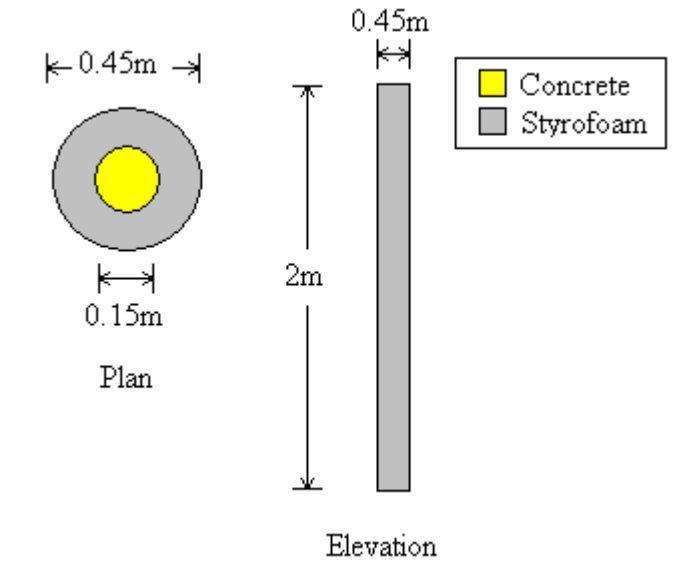

Figure 3 The base geometry reported by Lautz, plan and elevation views (not to scale).

When solving inverse problems, it is of critical importance that the methodology be robust in the presence of noisy observed data. For many of the experiments presented herein, artificial noise was added to the simulated target temperatures as

$$T_{t,s}^{error} = T_{t,s}^{exact}(1+\delta * \max(T) * \upsilon)\,. \qquad (22)$$

Where $T_{t,s}^{error}$ is the temperature including noise at the s^{th} sensor and the t^{th} time step, $T_{t,s}^{exact}$ is the simulated temperature at the s^{th} sensor and the t^{th} time step without noise, δ is a parameter used to determine the relative magnitude of the nose, $\max(T)$ is the maximum temperature recoded at any sensor over all time, and υ is a normally distributed random variable with unit variance and zero mean. This formulation of noise was found to produce reasonable deviations from the exact temperature profile.

In all forthcoming examples, the parameters are presented in normalized units to more clearly show the relative ability of the algorithm to capture different aspects of the problem. Modified convection coefficients, and parameters in the $\alpha(t)$ and

$\gamma(t)$ functions were replaced with normalized values. This transformation is in the form $p_i = \Upsilon_j \Pi_i : p_i \in (0,1)$, where p_i is the normalized parameter value, Π_i is the real parameter value and Υ_j is the scaling factor for that parameter type. Table 1 shows the value of Υ_j for each type of parameter.

Table 1 Parameter scaling factors

	Υ_j	Units of unscaled value
Modified convection coefficient	7.0922E-6	m/s
Thermal Diffusivity Point	5.6737E-7	m^2/s
Internal Heat Generation	6.6667E-3	K/s

Example Set 1: 1D Models With Exponential Decaying Heat Generation

The first set of example problems were performed using the 1D geometry shown in Figure 4. These examples used temperature sets generated using the exponentially decaying heat generation function shown in Figure 5 and the decreasing thermal diffusivity shown in Figure 6. The target temperatures were generated using the convective boundary conditions shown in Figure 4. When the boundary conditions were searched for, these became target values as well.

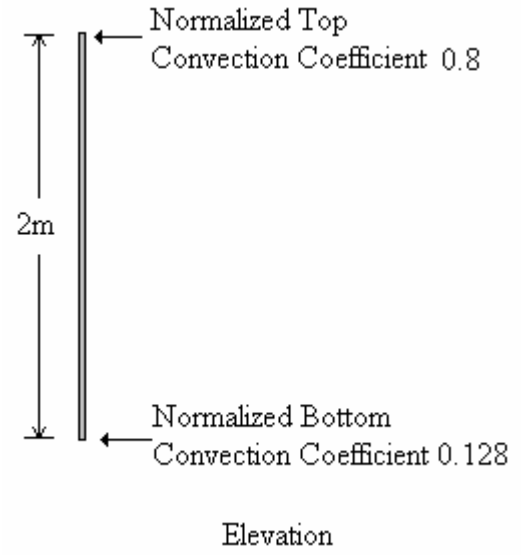

Figure 4 Schematic of the geometry and boundary conditions used for the 1D model.

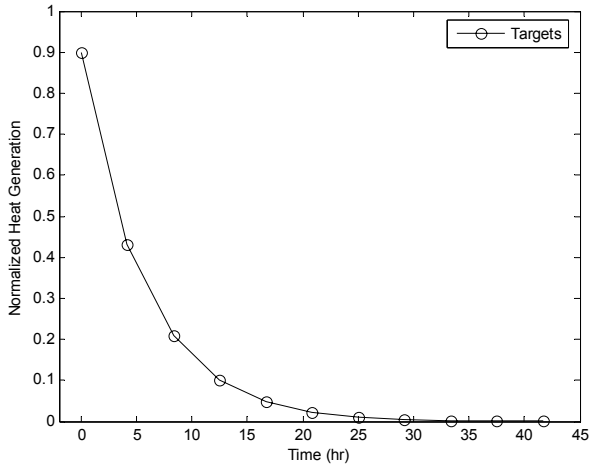

Figure 5 Exponentially decaying internal heat generation target function.

Two distributions of sensor positions were used, five sensors distributed uniformly along the length of the model, as shown in Figure 7, and the sensor configuration shown in Figure 8, where four sensors were located near the top and one sensor was at the bottom of the model. These configurations are hereafter referred to as "uniform" and "biased" sensor configuration, respectively. For some of the runs

random noise was added as shown in Equation (22). Table 2 summarizes the runs presented in this section.

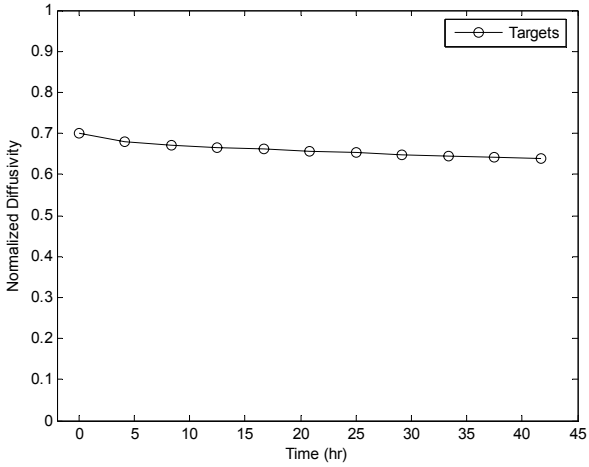

Figure 6 Decreasing thermal diffusivity target function.

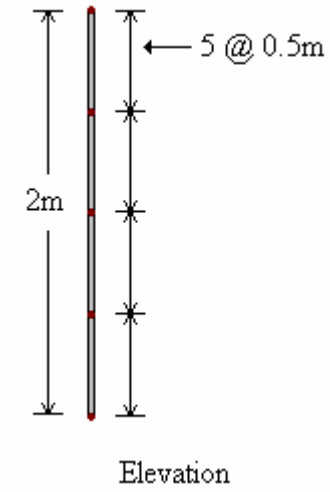

Figure 7 Schematic of the 1D model showing the "uniform' sensor locations.

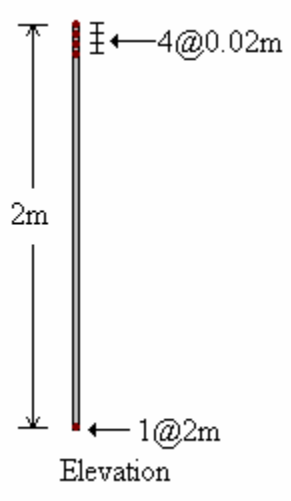

Figure 8 Schematic of the 1D model showing the "biased" sensor locations.

Table 2 Summary of runs presented in this section

Test Label	**Dimension Of Model**	**Noise** δ	**Diffusivity**	**Heat Generation**	λ_1	**Sensor Position**	**BC's Searched**
A	1D	0	Decreasing	Exp. Decay	0	Biased	None
B	1D	0	Decreasing	Exp. Decay	$10E^{-3}$	Uniform	None
C	1D	0	Decreasing	Exp. Decay	$10E^{-3}$	Biased	None
D	1D	0.01	Decreasing	Exp. Decay	$10E^{-3}$	Biased	None
E	1D	0.01	Decreasing	Exp. Decay	$10E^{-3}$	Biased	Top
F	1D	0.01	Decreasing	Exp. Decay	$10E^{-3}$	Biased	Top & Bottom

Table 3 Summary of the results of the runs in this section.

Test Label	**Number Run** n	$\frac{1}{n}\sum_{i=1}^{n} E_p(\vec{M}_i)$	$\frac{1}{n}\sum_{i=1}^{n} E_T(\vec{M}_i)$
A	10	0.0122	3.3881
B	10	0.0032	3.1544
C	10	0.0022	1.9150
D	10	0.0021	3.9229
E	10	0.0030	3.9919
F	10	0.0089	5.5034

Figures 9-20 show the results from each of the runs in this section; Table 3 summarizes the temperature and parameter error (Equations (17) and (18)) for each of these runs.

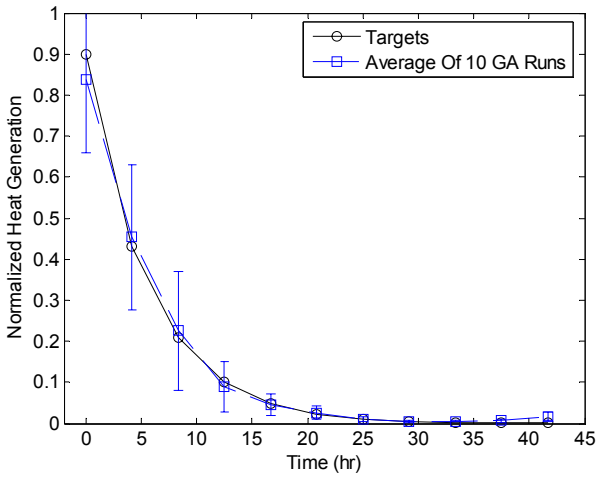

Figure 9 Heat generation results from Test A, mean and standard deviation (error bars).

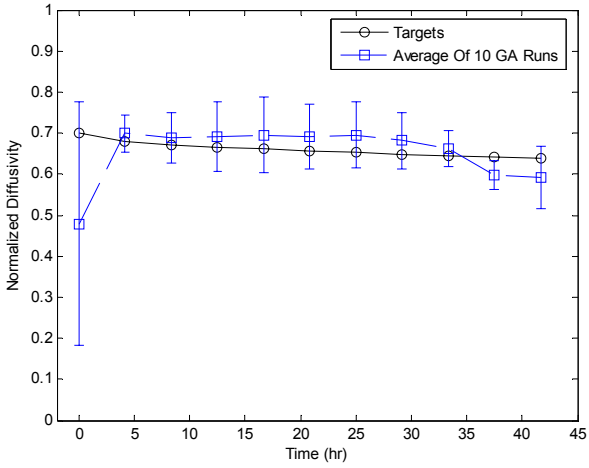

Figure 10 Thermal diffusivity results from Test A, mean and standard deviation (error bars).

Test A, which used sensor positions biased toward the top of the test model, but did not use any regularization, is shown in Figures 9 and 10. The mean estimate for

internal heat generation was accurate, but the standard deviation of the results was high. The accuracy of the thermal diffusivity was lower than that of the heat generation; this is because in this configuration, heat generation has a larger effect on the temperatures than thermal diffusivity. The lack of accuracy in the thermal diffusivity found by the algorithm at early times was expected, since values at the very early stage do not strongly affect temperatures at later stages.

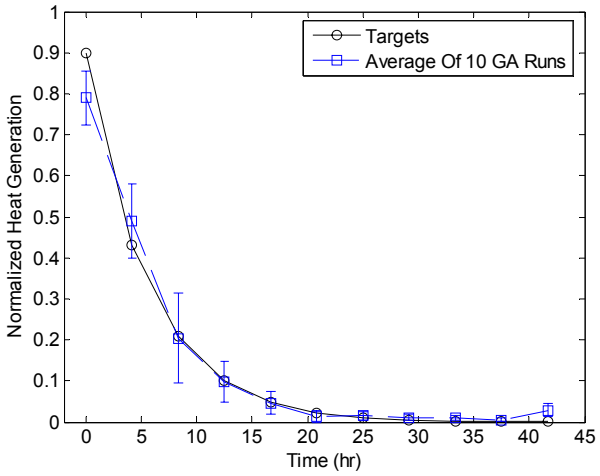

Figure 11 Heat generation results from Test B, mean and standard deviation (error bars).

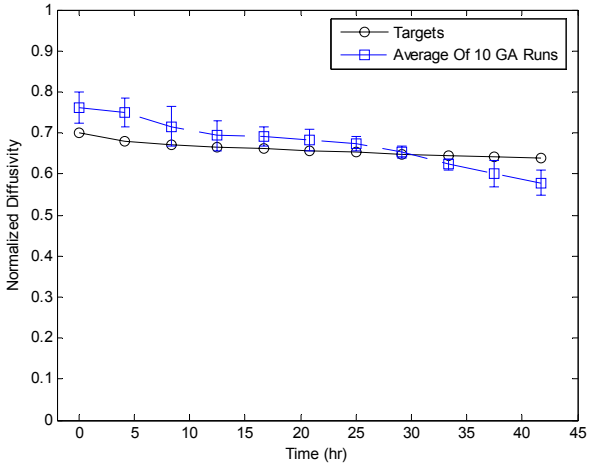

Figure 12 Thermal diffusivity results from Test B, mean and standard deviation (error bars).

In Test B, shown in Figures 11 and 12, a uniform distribution of sensors was used along with first-order regularization. The resulting inferred heat generation and diffusivity functions have significantly lower standard deviations. Additionally, the uncertainly in the first diffusivity point is reduced, as the error gradient with respect to that point is increased due to the added first-order regularization term. Since the temperatures are functions of the integral of the heat generation and diffusivity functions (integrals are smoothing operators), as shown by Equation (1), similar temperatures are created by parameter sets which fluctuate around the correct parameter values, overestimating or underestimating the solution. Regularization improves the performance of the algorithm by penalizing high frequency oscillations which may produce similar temperatures but have non-physical material behavior, see Colaco et. al [11] for a through treatment. From Table 3 it can be observed that the results display lower errors for both $\alpha(t)$ and $\gamma(t)$ compared to Test A.

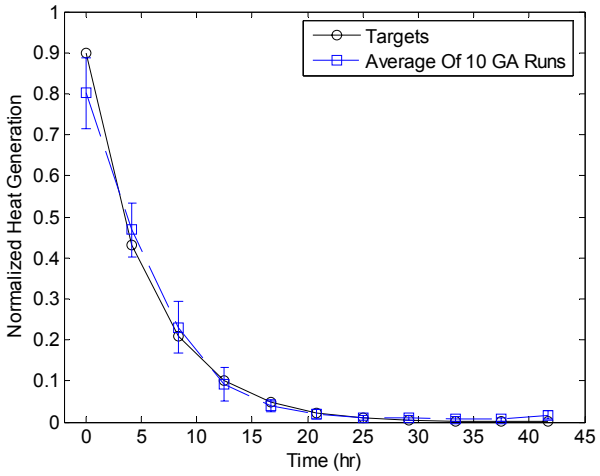

Figure 13 Heat generation results from Test C, mean and standard deviation (error bars).

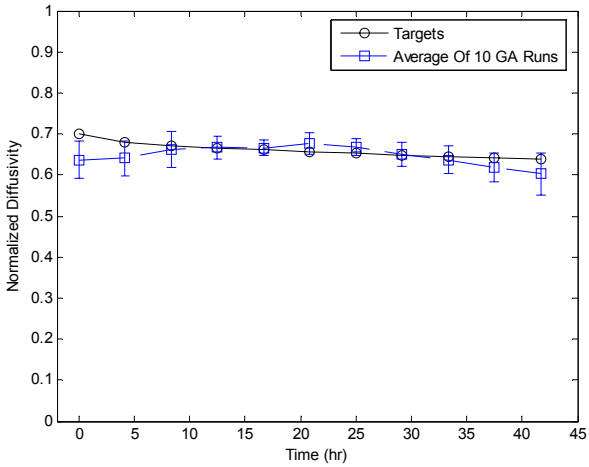

Figure 14 Thermal diffusivity results from Test C, mean and standard deviation (error bars).

Test C, shown in Figures 13 and 14 used biased sensor positions and first order Tikhonov regularization. Compared to Test B, the accuracy of both the heat generation and thermal diffusivity was improved and the variability of the results was also reduced. Table 3 shows that Test C improved upon Test B in terms of both temperature and parameter error. This shows that the locations of the sensors have a significant effect on the ability of the algorithm to find optimal solutions. Notice that the diffusivity solution was significantly improved, diffusivity has a strong affect on the temperature gradients near the ends, thus the clustering of sensors near this temperature gradient increases the sensitivity of the error function to diffusivity, leading to more accurate parameter identification. The improvements in the heat generation identification were apparent as well, but were not as significant.

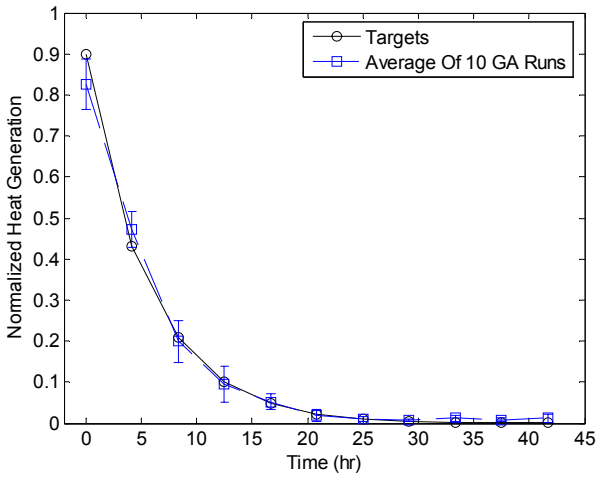

Figure 15 Heat generation results from Test D, mean and standard deviation (error bars).

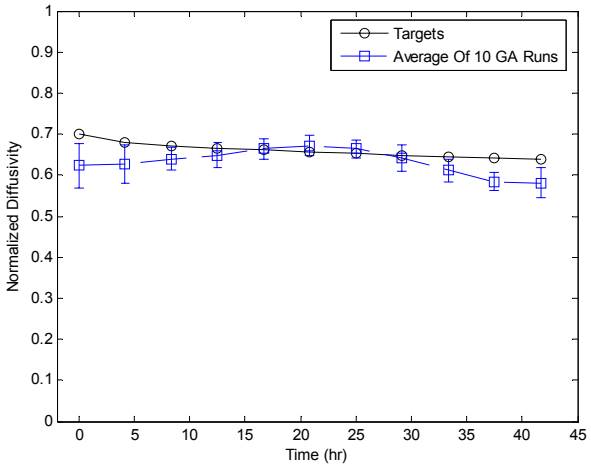

Figure 16 Thermal diffusivity results from Test D, mean and standard deviation (error bars).

In Test D, noise was added to the target temperatures with $\delta = 0.01$, the results are shown in Figures 15 and 16. Table 3 shows that, as expected, the addition of noise to the target temperatures increased the temperature error calculated by the algorithm. However, an interesting result is that the parameter error is slightly decreased. The phenomena has been observed before in the case of inverse problems, see for example the work of Constable [21]. The main effect which Constable reported to cause this

phenomena was that the noise increases the relative importance of the temperature error over the first-order regularization term in Equation (23), as the model can no longer minimize the temperature error.

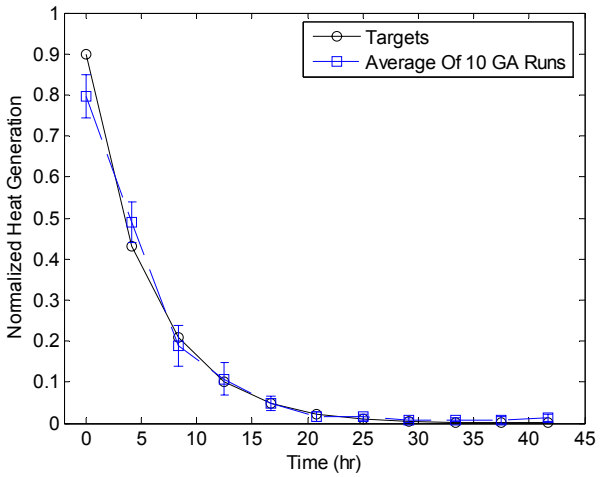

Figure 17 Heat generation results from Test E, mean and standard deviation (error bars).

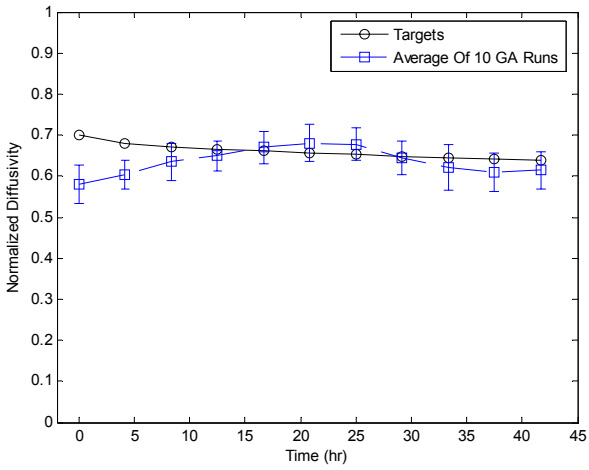

Figure 18 Thermal diffusivity results from Test E, mean and standard deviation (error bars).

Table 4 Modified convection coefficient at top found in Test E

	Target	Mean	Std. Dev
Top	0.8	0.763847	0.017369

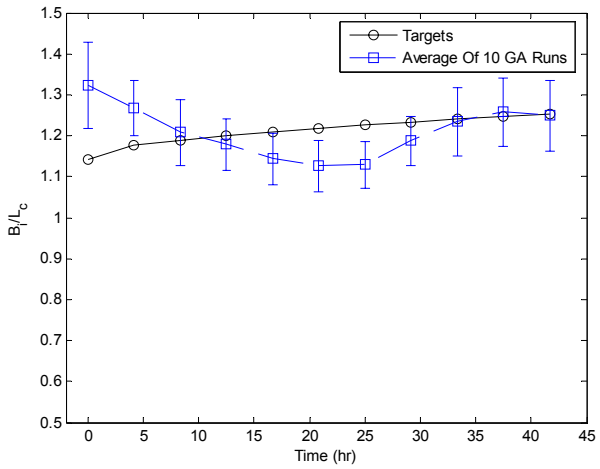

Figure 19 $\frac{B_i(t)}{L_c}$ results from Test E mean and standard deviation (error bars)

Test E investigated the ability of the algorithm to identify convective boundary conditions simultaneously with internal heat generation and thermal diffusivity. The modified convection coefficient at the top of the model was assumed unknown and was included in the search space. The results are shown in Figures 17, 18 and Table 4. The modified convection coefficient and heat generation function were identified with a good degree of accuracy. However, the accuracy of the thermal diffusivity solution was degraded as compared to the previous cases; Table 3 shows that the temperature error was not greatly increased, however, indicates that the algorithm was not trapped in a local minimum. This further indicates that introducing the convection coefficient in the search space affected the observability of the thermal diffusivity. This result is clear when Equation (2), repeated here, is observed.

$$\alpha(t)\nabla T\cdot\hat{n}=\eta\left(T_e-T\right),\quad \text{on } \Gamma_q$$

Thus at the boundary the behavior of the solution is governed by $\frac{\eta}{\alpha(t)}$ which is recognized as $\frac{B_i(t)}{L_c}$, where $B_i(t)$ is the dimensionless Biot number and L_c is the characteristic length, often defined as the ratio of the surface area to the volume of the

body [22] . Thus at the boundary, $\alpha(t)$ and η are under-determined. Figure 19 shows a plot of $\frac{B_i(t)}{L_c}$, it shows that this parameter was found with similar accuracy as $\alpha(t)$.

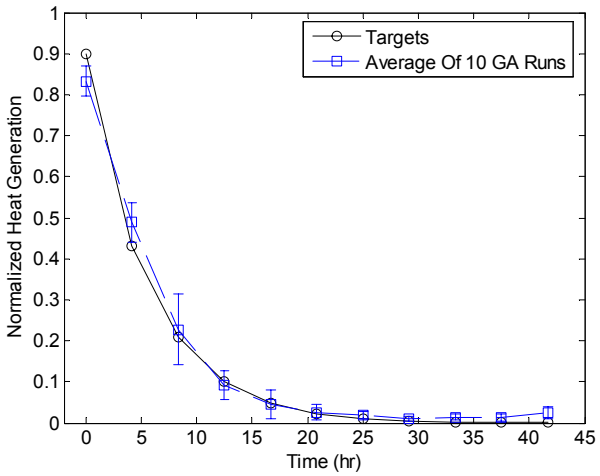

Figure 20 Heat generation results from Test F, mean and standard deviation (error bars).

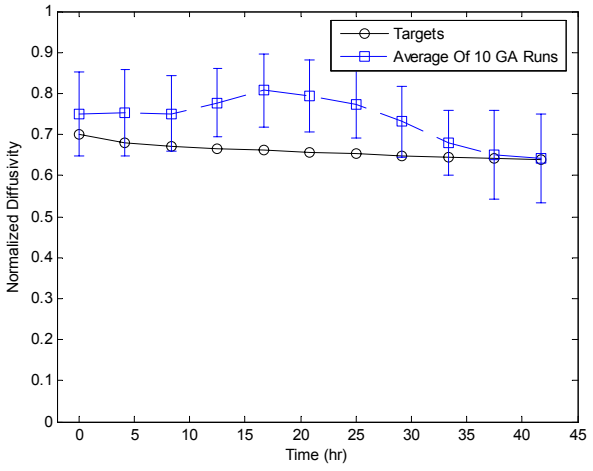

Figure 21 Thermal diffusivity results from Test F, mean and standard deviation (error bars).

Table 5 Modified convection coefficients at top and bottom found in Test F

	Target	Mean	Std. Dev
Top	0.8	0.899508	0.093333
Bottom	0.128	0.153574	0.024219

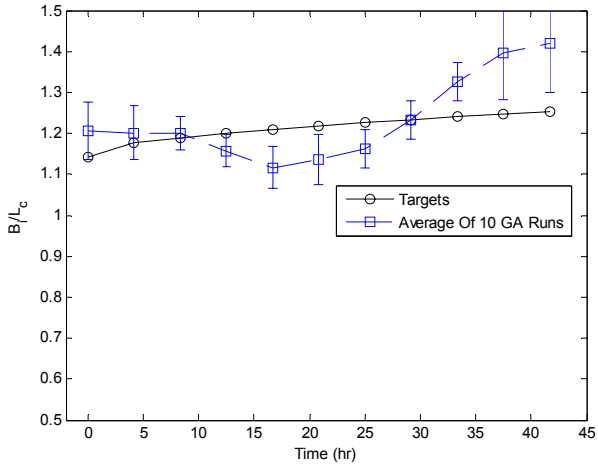

Figure 22 $\frac{B_i(t)}{L_c}$ results at the top from Test F mean and standard deviation (error bars)

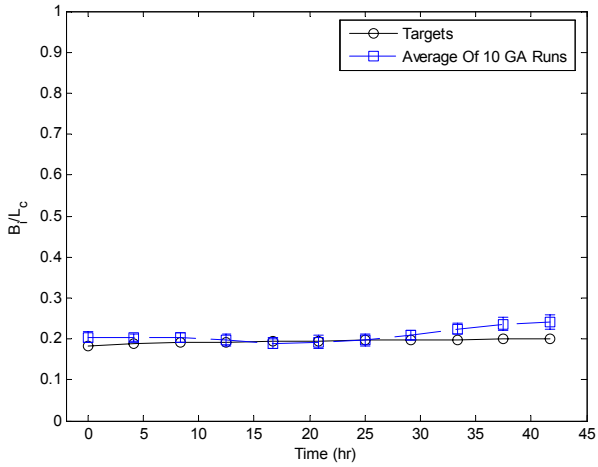

Figure 23 $\frac{B_i(t)}{L_c}$ results at the bottom from Test F mean and standard deviation (error bars)

In Test F, both the top and bottom modified convection coefficients were assumed to be unknown in addition to the thermal diffusivity and the heat generation functions. It

can be noticed in Figures 20 and 21, and Table 5 that the increase in the search space degraded the accuracy of the estimated thermal diffusivity function and increased the variance of all the search parameters compared to Test E. Table 3 shows that Test F has the largest parameter and temperature errors of any of the tests with the exponential decaying heat generation and first order regularization. These results indicate that the parameter space increased the difficulty of the optimization problem, preventing the GA from finding a global optimum in the number of generations used in this test. It is possible that improved results could be achieved with a longer optimization run. Figures 22 and 23 show the results for $\frac{B_i(t)}{L_c}$ at the top and the bottom of the model, respectively; they show that the solution very accurately identified $\frac{B_i(t)}{L_c}$ on the bottom, the results for $\frac{B_i(t)}{L_c}$ for the top of the model were degraded as compared to Test F.

Example Set 2: 1D Models With Peaked Heat Generation Function

In order to explore the ability of the algorithm to identify other heat generation target functional forms, a second heat generation function was tested. The new target heat generation function, which is peaked in the middle, is shown in Figure 24. The thermal diffusivity and the biased sensor configuration remained the same as in the previous tests and are shown in Figures 6 and 8 respectively. Table 6 summarizes the examples presented in this section, and Table 7 summarizes the temperature and parameter error as calculated by Equations (17) and (18).

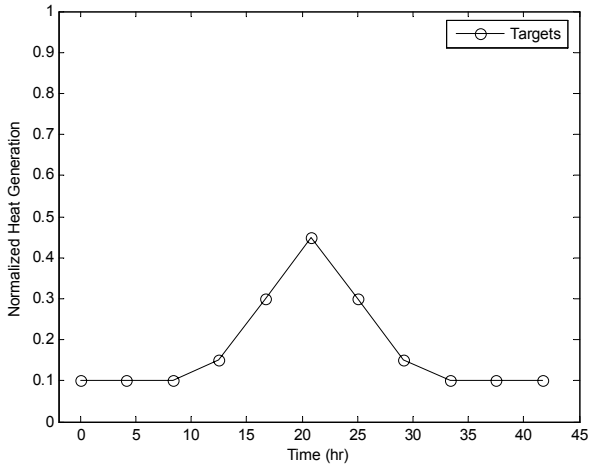

Figure 24 Peaked internal heat generation target function

Table 6 Summary of runs presented in this section

Test Label	**Dimension Of Model**	**Noise** δ	**Diffusivity**	**Heat Generation**	λ_1	**Sensor Position**	**BC's Searched**
G	1D	0%	Decreasing	Peaked	$10E^{-3}$	Biased	None
H	1D	1%	Decreasing	Peaked	$10E^{-3}$	Biased	None

Table 7 Summary of the results of the runs in this section.

Test Label	**Number of Runs** n	$\frac{1}{n}\sum_{i=1}^{n} E_p(\vec{M}_i)$	$\frac{1}{n}\sum_{i=1}^{n} E_T(\vec{M}_i)$
G	10	0.0056	1.7810
H	10	0.0036	3.5011

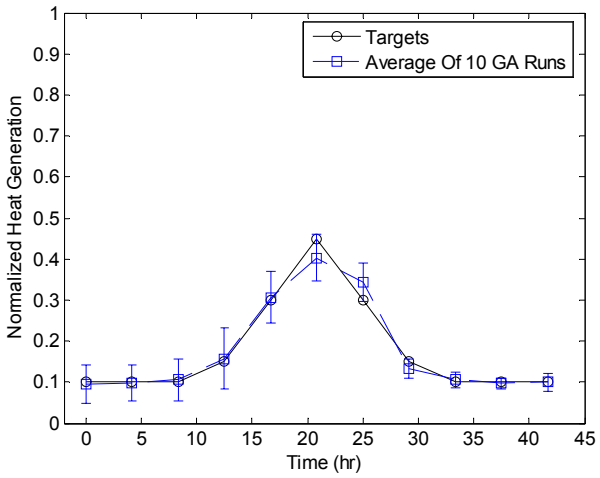

Figure 25 Heat generation results from Test G, mean and standard deviation (error bars).

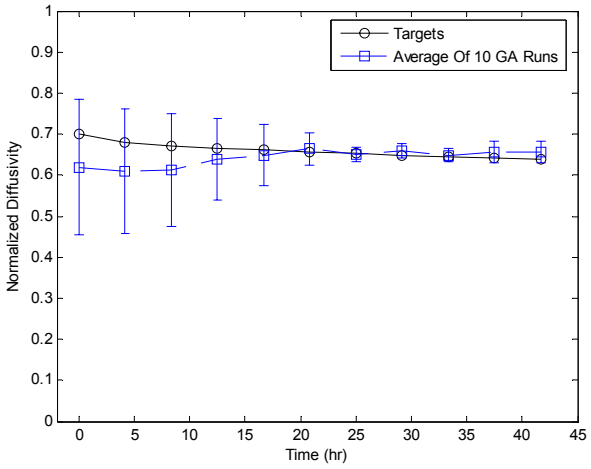

Figure 26 Thermal diffusivity results from Test G, mean and standard deviation (error bars).

Test G was the baseline test of the peaked-heat target heat generation function. The target heat generation was accurately identified as shown in Figure 25. However, the diffusivity was not accurately identified and had very high variance, in the early stages of the process as shown in Figure 26. This result shows that the heat generation function affects the ability of the algorithm to find the diffusivity function. Heat generation affects the observability of the diffusivity coefficient by changing the shape

and timing of temperature profiles in the column, the error is more sensitive to diffusivity when there are large gradients in temperature throughout the column.

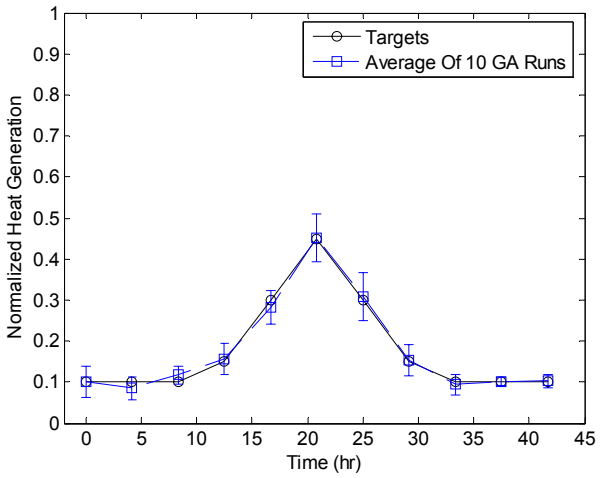

Figure 27 Heat generation results from Test H, mean and standard deviation (error bars).

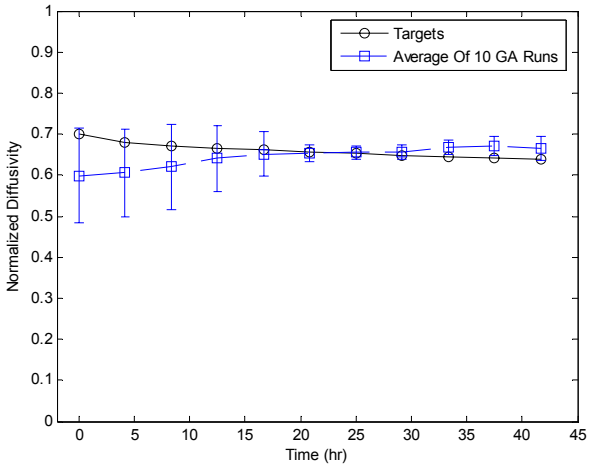

Figure 28 Thermal diffusivity results from Test H, mean and standard deviation (error bars).

In Test H random noise with $\delta = 0.01$ was added to the target temperature data from Test G, the results are shown in Figures 27 and 28. As found in Tests C and D, Table 7 shows that the addition of noise increased the temperature error but decreased the

parameter error; in this case the decrease of the parameter error was very significant. This improvement can be explained with the same reasoning as was explained for the parameter improvement observed in Test D.

Example Set 3: 1D Model With Highly Nonlinear Diffusivity Function

In order to explore the ability of the algorithm to identify other thermal diffusivity target functions, a second, highly nonlinear, thermal diffusivity function was tested. The new target function is shown in Figure 29. The heat generation was the same exponentially decaying heat generation function shown in Figure 5, and the sensor locations were the biased locations shown in Figure 8. Table 8 summarizes the examples presented in this section, and Table 9 summarizes the temperature and parameter error as calculated by Equations 17 and 18.

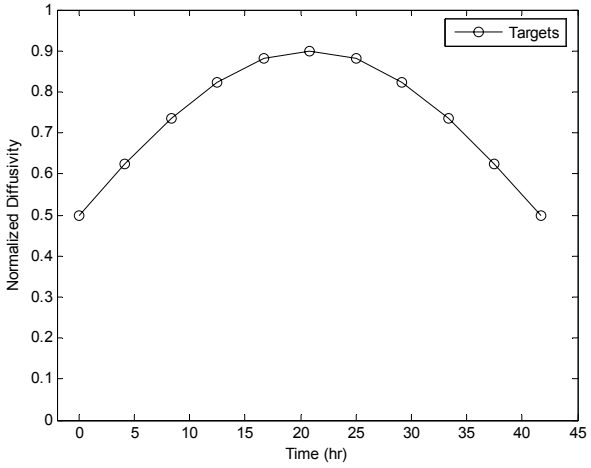

Figure 29 Parabolic thermal diffusivity target function.

Table 8 Summary of runs presented in this section

Test Label	Dimension Of Model	Noise δ	Diffusivity	Heat Generation	λ_1	Sensor Position	BC's Found
I	1D	0%	Parabolic	Exp. Decay	0	Biased	None

Table 9 Summary of the results of the runs in this section.

Test Label	**Number Run** n	$\frac{1}{n}\sum_{i=1}^{n} E_p(\vec{M}_i)$	$\frac{1}{n}\sum_{i=1}^{n} E_T(\vec{M}_i)$
I	10	0.0080	12.5393

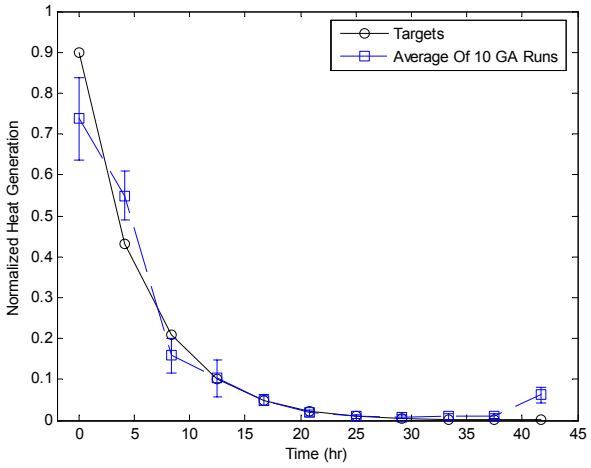

Figure 30 Heat generation results from Test I, mean and standard deviation (error bars).

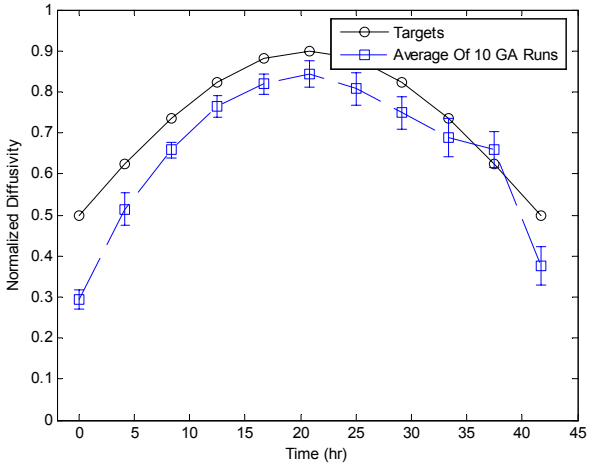

Figure 31 Thermal diffusivity results from Test I, mean and standard deviation (error bars).

The results from Test I are shown in Figures 30 and 31. Although the thermal diffusivity identified was not highly accurate, the correct trend was found. The heat

generation identified in this run is among the least accurate of all the runs. Note that to identify this highly nonlinear diffusivity, no regularization was used, as poor results were found with regularization, this is because the error function is relatively insensitive to diffusivity, regularization only serves to force the model the prefer non-oscillating diffusivities. These results may be able to be improved with additional sensors and/or different sensor layouts. These options were not investigated for the sake of brevity.

Example Set 4: 2D Axisymmetric Models with Realistic Heat Generation

The last set of example problems were performed using the 2D-Axisymmetric geometry shown in Figure 32. These examples all used temperature sets generated using the "realistic" heat generation function shown in Figure 33 and the six-point "short" decreasing thermal diffusivity shown in Figure 34. The target temperatures were generated using the convective boundary conditions shown in Figure 32, when the boundary conditions were searched for these became the target values as well.

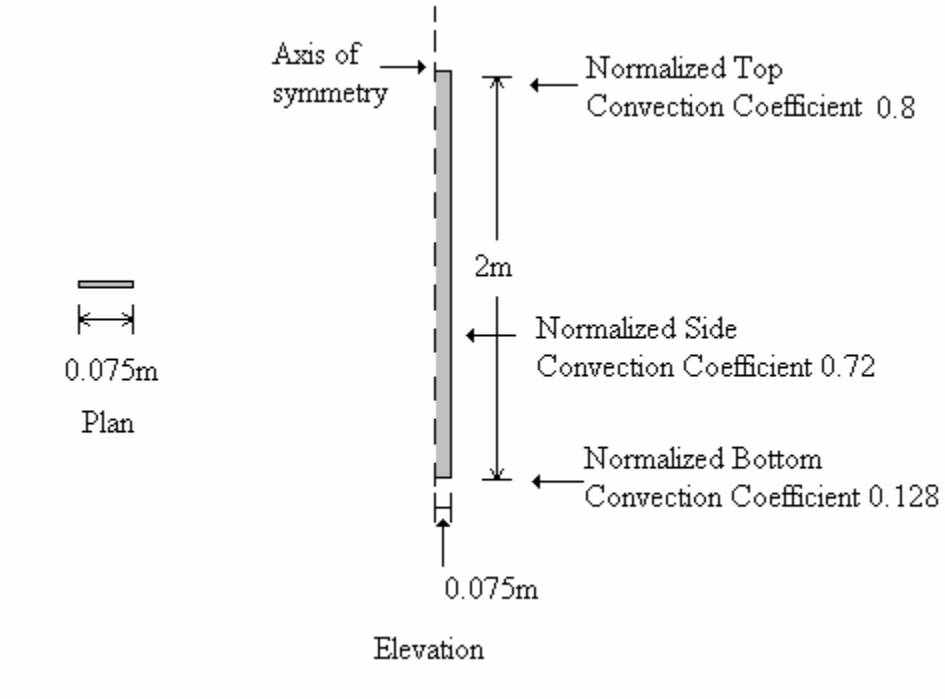

Figure 32 Plan and elevation schematics of the 2D-axisymmetric model, showing target modified convection coefficients.

Note: Not to Scale.

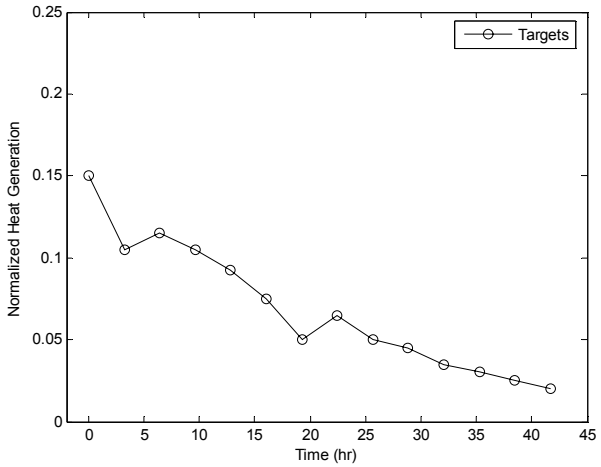

Figure 33 Simulated concrete internal heat generation target function

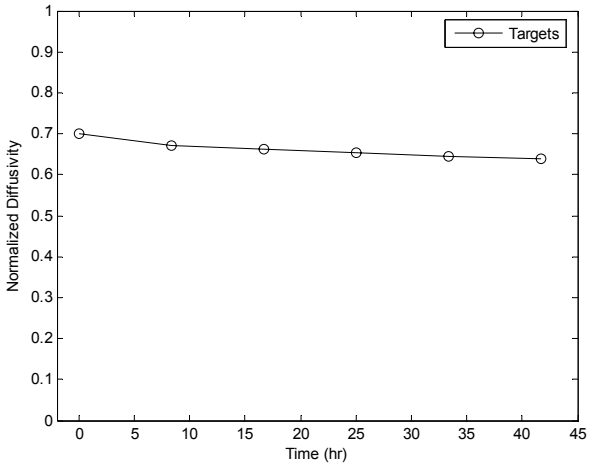

Figure 34 Short (only 6 point) diffusivity function

The sensor locations changed between the 1D and 2D model as well, the sensors were located on the surface for Test J, and in three rows equally spaced through the column for Test K. These configurations are shown in Figures 35 and 36. For these runs random noise was added as shown in Equation (22). Table 10 summarizes the runs presented in this section and Table 11 summarizes the temperature and parameter error for those runs as calculated using Equations (17) and (18).

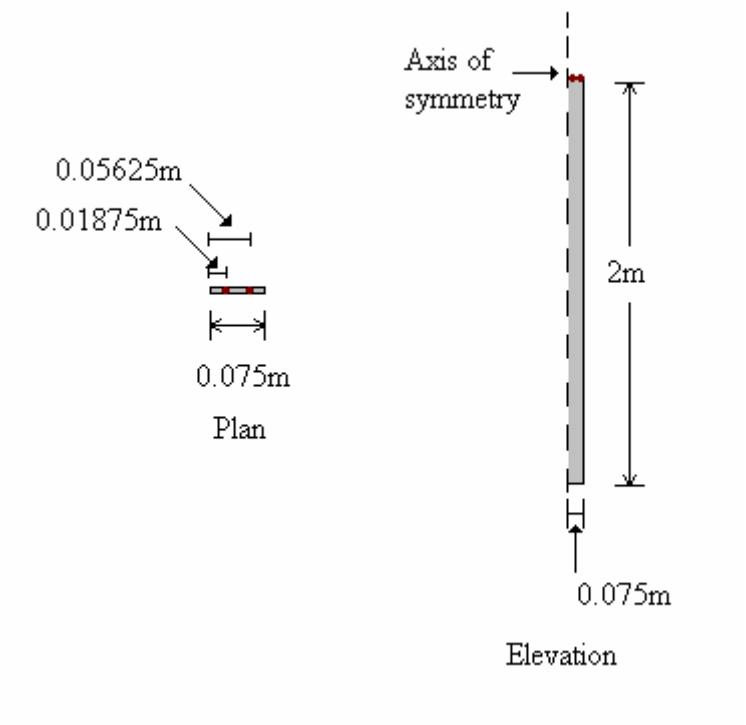

Figure 35 Sensors for the surface sensor configuration.

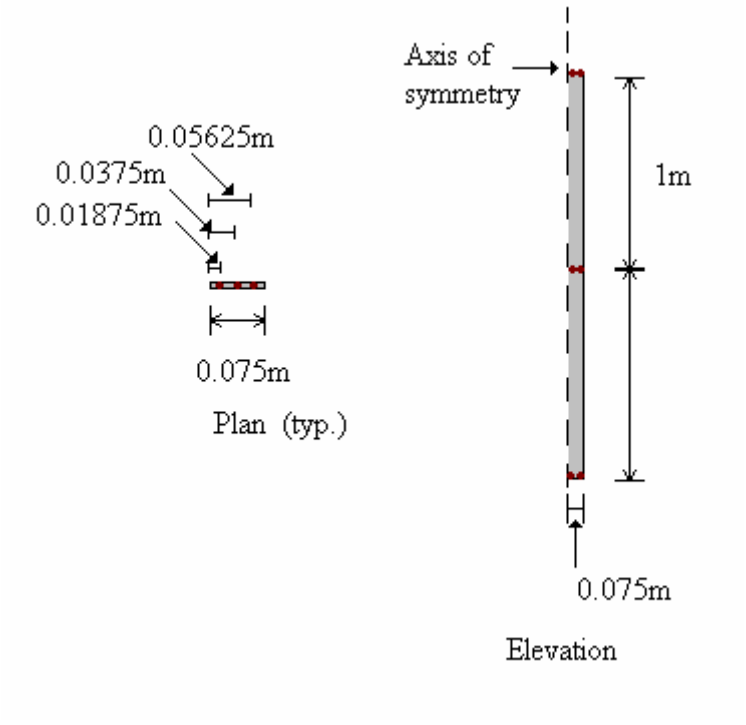

Figure 36 Sensors for the "three row" configuration, nine sensors arranged in three rows of three.

Table 10 Summary of runs presented in this section

Test Label	**Dimension Of Model**	**Noise** δ	**Diffusivity**	**Heat Generation**	λ_1	**Sensor Position**	**BC's Found**
J	2D	1%	Short	Realistic	$10E^{-4}$	Surface	None
K	2D	1%	Short	Realistic	$10E^{-5}$	Three Row	Total

Table 11 Summary of the results of the runs in this section.

Test Label	**Number Run** n	$\frac{1}{n}\sum_{i=1}^{n} E_p(\vec{M}_i)$	$\frac{1}{n}\sum_{i=1}^{n} E_T(\vec{M}_i)$
J	10	0.0005	0.0991
K	10	0.0111	0.0220

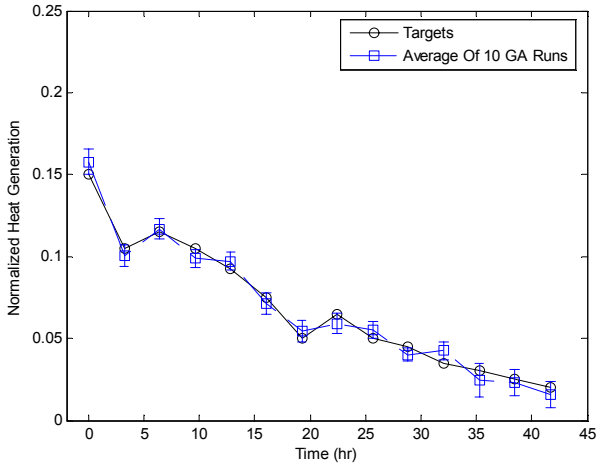

Figure 37 Heat generation results from Test J, mean and standard deviation (error bars).

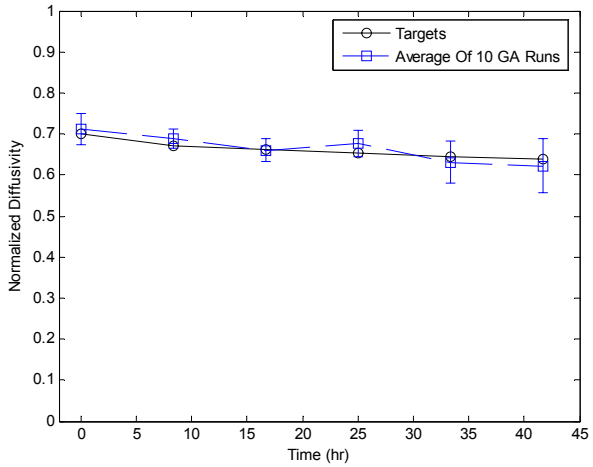

Figure 38 Thermal diffusivity results from Test J, mean and standard deviation (error bars).

Test J, shown in Figures 37 and 38, tested the ability of the algorithm to identify a heat generation which was adapted from Bye [23] and a diffusivity similar to previous tests using only surface temperatures with a 2D axisymmetric model and noise. The resulting heat generation and conductivities are very accurate with very low variance. This is a surprising and interesting result as one could have erroneously guessed that this problem was ill-posed due to the few sensors used.

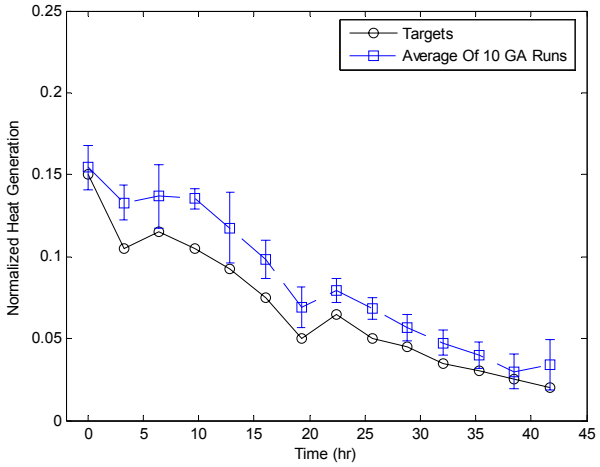

Figure 39 Heat generation results from Test K, mean and standard deviation (error bars).

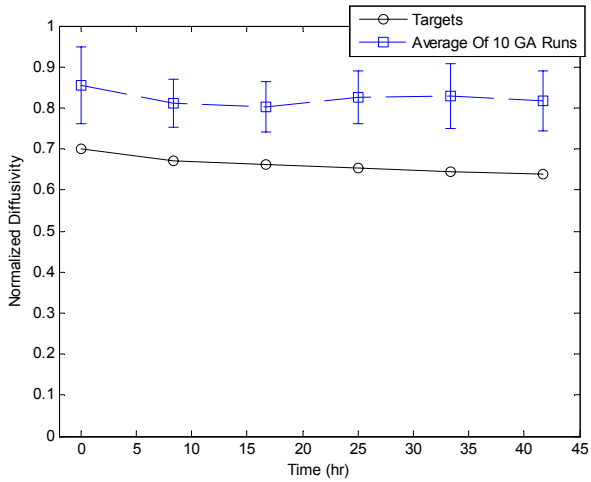

Figure 40 Thermal diffusivity results from Test K, mean and standard deviation (error bars).

Table 12 Modified convection coefficients found in Test K

	Target	Mean	Std. Dev
Top	0.8	0.956135	0.02955
Side	0.72	0.928083	0.059627
Bottom	0.128	0.156412	0.013688

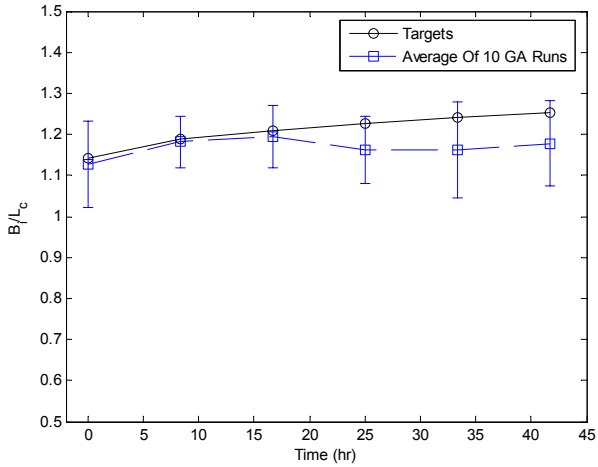

Figure 41 $\frac{B_i(t)}{L_c}$ results at the top from Test K mean and standard deviation (error bars)

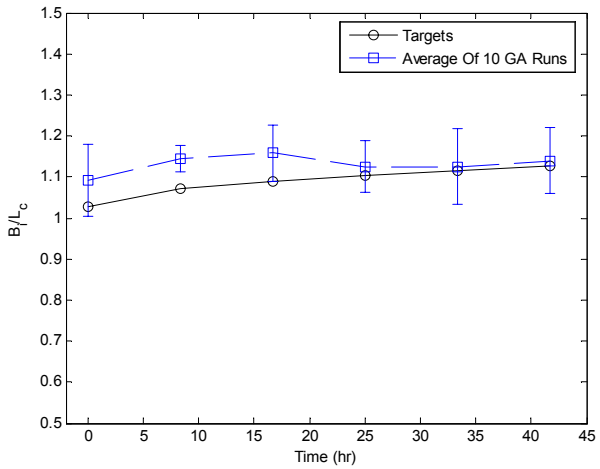

Figure 42 $\frac{B_i(t)}{L_c}$ results at the side from Test K mean and standard deviation (error bars)

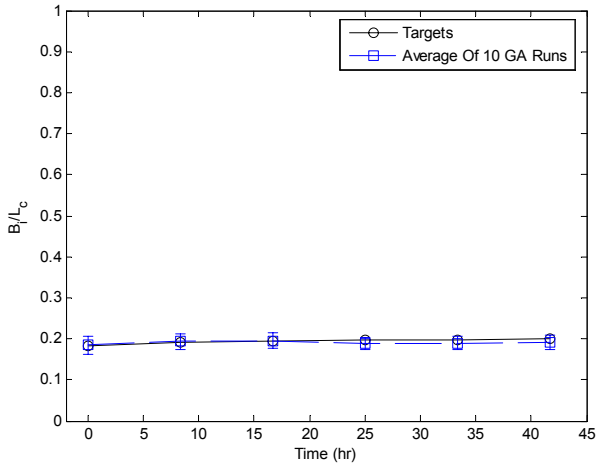

Figure 43 $\frac{B_i(t)}{L_c}$ results at the bottom from Test K mean and standard deviation (error bars)

Test K is similar to Test J, but all three sides of the model are assumed to have an unknown modified convection coefficient on all three sides which is also being searched for**.** The heat generation and diffusivity results from this run, shown in Figures 36 and 37 are significantly less accurate than Test J, and the convection coefficients, shown in Table 13 were not identified well either. All the parameters

were consistently over-estimated, with values significantly away from the target values, interestingly while the parameter error increased very significantly compared to Test J, the temperature error was lower, suggesting that this problem is ill-posed, and that the parameter sets found did produce temperatures similar to the target system. Figures 38-40, which show $\frac{B_i(t)}{L_c}$ for the top, side and bottom of the model, support the conclusion that the problem as formulated was ill-posed. Although diffusivity and the convection coefficients were consistently over-estimated, $\frac{B_i(t)}{L_c}$ was found with much higher accuracy. This finding suggests that for this problem $\frac{B_i(t)}{L_c}$ was identifiable, but the individual components of it were not.

CHAPTER 4

CONCLUSIONS

Conclusions

In this thesis a methodology was introduced to solve the IHTP using a genetic algorithm. The algorithm produced accurate results, reliably identifying internal heat generation, thermal diffusivity, and modified convection coefficients simultaneously, even in the presence of noise. Comparing the results of Test A with Test C, it was shown that the accuracy was improved by the use of first order Tikhonov regularization. Comparisons of Tests C and D and Tests G and H showed the interesting results that zero-mean noise in the target temperature data improved the accuracy of the resulting parameter sets and the cause of this improvement was surmised. Additionally, it was shown that with realistic concrete internal heat generation, and a 2D axisymmetric model, even in the presence of noise, the algorithm could effectively identify transient heat generation and diffusivity with just surface temperatures. It was demonstrated that searching for convective boundary conditions simultaneously with heat generation and diffusivity is sometimes possible, but they can be underdetermined, as the behavior at the boundary depends on the quotient of thermal diffusivity and the convection coefficient (i.e. Biot number). In the case that the individual terms are not identifiable, it was shown that the Biot number may be identified instead.

REFERENCES

1. Lautz, C.H., *Estimating Compressive Strength and Thickness of Concrete Based on Surface Temperature*, in *Civil and Environmental Engineering*. 2004, Cornell University: Ithaca, NY. p. 410.
2. Gil Peaez, J.J., Just-Agosto, F.A., Serrano, D., and Shafiq, B, *Deteccion de Daño Usando Transferencia de Calor por Conducción.* Revista Internacional de Desastres Naturales, Accidentes e Infrastructura Civil, 2003. **3**(2): p. 129-142.
3. Giedt, W.H., *Determination of transient temperatures and heat transfer at gas-metal interface applied to 40-mm gun barrel.* Jet Propulsion, 1955. **25**(4).
4. Su, J., Hewitt, G.F., *Inverse Heat Conduction Problem of Estimating Time-Varying Heat Transfer Coefficient.* Numerical Heat Transfer, Part A, 2004. **45**: p. 777-789.
5. Truffart, B., Jarny, Y., Delaunay, D., *A General Optimization Algorithm to Solve 2-D Boundary Inverse Heat Conduction Problems Using Finite Elements.* Inverse Problems in Engineering: Theory and Practice, 1993.
6. Al-Najem, N.M., *Inverse Heat Generation Problem in a Hollow Cylinder.* Inverse Problems in Engineering: Theory and Practice, 1993.
7. Abou, K.R., Jarny, Y., *Estimation of Heat Sources Within two Dimensional Shaped Bodies.* Inverse Problems in Engineering: Theory and Practice, 1999.
8. Jang, H.Y., Tuan, P.C., Chen, T.C., Chen, T.S., *Input Estimation Method Combined With The Finite-Element Scheme To Solve IHCP Hollow Cylinder*

Inverse Heat Conduction Problems. Numerical Heat Transfer, Part A, 2006. **50**: p. 263-280.

9. Rodrigues, F.A., Orlande, H.R.B., and Dulikravich, G.S., *Simultaneous Estimation of Spatially Dependent Diffusion Coefficient and Source Term in a Nonlinear 1D Diffusion problem.* Mathematics and Computers in Simulation, 2004. **66**(4-5): p. 409-424.
10. Silva, A.J., Ozisk, M.N., *The estimation of space and time dependent strength of a volumetric heat source in a one-dimensional plate.* Int. J. Heat Mass Transfer, 1993. **37**(6): p. 909-915.
11. Colaco, M.J., Orlande, H.R.B., Dulikravich, G.S., Rodrigues, F.A. *A Comparison of Two Solution Techniques for the Inverse Problem of Simultaneously Estimating the Spatial Variations of Diffusion Coefficients and Source Terms*. in *2003 ASME International Mechanical Engineering Congress*. 2003. Washington, D.C.: ASME.
12. Reddy, J.N., *An Introduction To Nonlinear Finite Element Analysis*. 2004, New York: Oxford University Press Inc. 463.
13. Alifanov, O.M., *Inverse Heat Transfer Problems.* 1994.
14. Marin, L. and D. Lesnic, *BEM first-order regularization method in linear elasticity for boundary identification.* Computer Methods in Applied Mechanics and Engineering, 2003. **192**(16-18): p. 2059-2071.
15. Holland, J.H., *Adaptation in Natural and Artificial Systems*. 1975, Ann Arbor, MI: University of Michigan Press.

16. Foster, N.F. and G.S. Dulikravich, *Three-dimensional aerodynamic shape optimization using genetic and gradient search algorithms.* Journal Of Spacecraft And Rockets, 1997. **34**(1): p. 36-42.

17. Ponterosso, P., et al., *Masonry arch collapse loads and mechanisms by heuristically seeded genetic algorithm.* Computer Methods in Applied Mechanics and Engineering, 2000. **190**(8-10): p. 1233.

18. Paul, C., H. Lipson, and F.J.V. Cuevas. *Evolutionary form-finding of tensegrity structures*. 2005. Washington, D.C., United States: Association for Computing Machinery, New York, NY 10036-5701, United States.

19. Goldberg, D.E., *Genetic Algorithms In Search, Optimization and Machine Learning*. 1989, Boston: Addison-Wesley. 412.

20. Mitchell, M., *An Introduction to Genetic Algorithms.* 1999.

21. Constable, S., *Comment on `Magnetotelluric appraisal using simulated annealing' by Dosso and Oldenburg.* Geophysical Journal International, 1991. **106**(2): p. 387-388.

22. Incropera, F.P., DeWitt, D.P., *Introduction to Heat Transfer*. Vol. 4. 2002, New York: John Wiley & Sons.

23. Bye, G.C., *Portland Cement - Composition, Production, and Properties*. 1983: Pergamon Press. 149.